A Method for Stabilizing Unstable Periodic Orbits in Dynamic Mode Atomic Force Microscopy

Hannes Wallner[1], Lukas Böttcher[2,3], Niklas Kruse[1], Wolfram Just[1], Ingo Barke[2,3], Sylvia Speller[2,3] & Jens Starke[1]
[1] *Institute of Mathematics, University of Rostock, 18051 Rostock, Germany*
[2] *Institute of Physics, University of Rostock, 18051 Rostock, Germany and*
[3] *Department Life, Light & Matter, University of Rostock, 18051 Rostock, Germany*
(Dated: January 10, 2025)

We present a non-invasive feedback-control scheme to access unstable periodic orbits in dynamic mode atomic force microscopy. By utilising this method we are able to explore the complete nonlinear frequency-response curves, including unstable branches between saddle-node bifurcations. The overall scheme is designed to be fast and derivative-free, which allows for simple experimental implementations. The control is closely related to Phase-Locked-Loop testing, a truncated Fourier discretization of periodic orbits and an adaptive filter for online signal demodulation. We demonstrate the feedback-control on various contact models for dynamic mode atomic force microscopy and would like to motivate for future laboratory experiments by elucidating software and corresponding hardware implementations in detail.

Keywords: atomic force microscopy (AFM), scanning force microscopy (SFM), unstable periodic orbits (UPO), frequency response curves (FRC), dynamic mode AFM, control-based continuation (CBC), phase-locked loop (PLL), experimental continuation, adaptive filtering, critical transitions

I. INTRODUCTION

In recent decades, a strive began to observe, understand and manipulate objects at the nanoscale. Consequently, different imaging techniques for the topography of surfaces were established. One option, the scanning tunneling microscope (STM), was introduced by Binnig and Rohrer in 1983 [1] and uses the tunneling current between a sharp conducting tip and a conducting sample to sense the surface of the sample on the atomic scale. Only three years later in 1986 Binnig, Gerber et. al [2] generalized the idea and invented the atomic force microscope (AFM), also known as scanning force microscope (SFM), which no longer was restricted to conductive materials. Instead of electron transport, its principle is based on tip-sample interaction forces. A commonly used operational mode of AFM is the dynamic mode, due to its short interaction times with the sample and thereby inherently less destructive behavior, as opposed to the contact mode, where the tip remains in a repulsive interaction permanently. In dynamic AFM a microcantilever is driven to oscillations above a sample. The dynamics of the tip, located at the end of the cantilever, are monitored by a laser and reflected onto a segmented photodiode and can in first approximation be described as a nonlinear driven damped harmonic oscillator. By demodulation of the displacement dynamics one can in general obtain surface properties.

New directions in dynamic mode AFM introduce multiharmonic excitation in order to reconstruct tip-sample interactions through Fourier mode mappings [3] or more recently by sparse identification of nonlinear dynamical systems (SINDy) [4, 5]. We would like to highlight, that the displacement dynamics of the tip under monoharmonic excitation is still not completely explored and might reveal features in order to gain further information on the interaction properties. This can be seen by varying the driving frequency adiabatically under constant forcing amplitude and tracking the solution, manifesting in multistable nonlinear frequency-response curves (FRC) that experimentally only include stable periodic orbits [6, 7]. As a result one observes jump-phenomena at bifurcation points, located at the end of the stable branches in the FRC. From theoretical works [8, 9] it is well established within the AFM-community, that an unstable branch of solutions, consisting of unstable periodic orbits (UPO) connects the saddle-node bifurcation points. Recently, successful stabilization of UPOs, with the here proposed control, have been reported in an actual AFM experiment [10]. Such new AFM methods could lead to novel spectroscopy and imaging methods due to the naturally unobtainable operating mode. Knowledge of the unstable branch can also be used to calibrate parameters of the system, as for example done in a nanoscopic Duffing oscillator [11] and in the context of atomic force microscope for the estimation of the tip radius [12].

The aim of this work is to take recent developments in the field of experimental continuation and present a stabilization technique for unstable periodic orbits in dynamic mode atomic force microscopy, that is suited not only for numerical continuation but in particular for a laboratory scenario. Therefore, we focus on a fast, derivative-free, model-free and non-invasive feedback control scheme that allows for tracking of nonlinear frequency response curves by changing the driving frequency. The paper is thereby structured as follows. First, we will shortly introduce dynamic mode atomic force microscopy. In section 2 we present concepts and algorithms that will be necessary for the implementation of the feedback-control law. In order to show that the scheme is able to stabilize periodic orbits on a vast variety of tip-sample interaction force models, in section 3 we apply the control-scheme numerically on a Duffing,

Lennard-Jones and Derjaguin-Muller-Toporov model, respectively, and show that intrinsic limitations seem reasonable. This paper is aimed to provide a solid base for experimental implementations, while actual laboratory experiments will remain the topic of separate publications.

II. METHODS

Generally, in the field of control-based continuation (CBC), several methods were developed, that enable stabilizing formerly unstable periodic solutions and therefore tracking them in different experimental scenarios without changing the solution itself. The underlying idea is to actively manipulate the original dynamics of the system by a feedback-control signal, which acts in such a way that we are able to reach the former unstable time invariant set [13, 14]. Once reached, the feedback-control signal vanishes and only the original dynamics remain, in other words the control scheme is so-called non-invasive [15–17]. One solely manipulates the linearization of the dynamical system and therefore stability around the time invariant set. In this manner, unstable branches in many scenarios such as pedestrian flows [18], Zeeman catastrophe machines [19], gene synthesis networks [20], neuronal states [21] etc. were obtained. In fact, experimental nonlinear response curves with unstable branches were measured with such methods for multiple forced nonlinear oscillators [14, 22–25]. An excellent introduction of experimental continuation can be found in the overview article [26], more recent adaptations that include adaptive control can be found in [27]. The challenge to apply these methods in dynamic mode atomic force microscopy can be boiled down to the requirement to operate at the spatial nanoscale, implying inherent noise contributions as well as the fast temporal dynamics. As shown for micro- and nanoelectromechanical systems (MEMS/NEMS), even stability of branches is often not sufficient to physically observe states on them, due to small basins of attraction [28]. Non-invasive feedback control can also be used to enlarge basins [29]. To illustrate these challenges we will shortly introduce dynamic mode atomic force microscopy.

A. Nonlinear Experiment - Dynamic Mode Atomic Force Microscopy

The overall setup consists of a microcantilever that is excited at the base by piezo actuators above a sample, in the near resonance regime of the first mechanical mode of the cantilever. The motion of the tip of the cantilever is tracked by a laser and segmented photodiode, see figure 1**a**), and is strongly influenced by nonlinear interaction forces between tip and sample, which can be characterized by long-range attractive van-der-Waals forces and short-range repulsive interactions. The nonlinearity of the force can thereby be adjusted by the separation s, that measures the distance between the tip of the cantilever and the sample in non driven case without interaction forces, see figure 1**a**). Under constant separation s and excitation amplitude F one can increase (forward sweep) or decrease (backward sweep) the driving frequency. By applying demodulation techniques on the time-dependent deflection voltage, which is proportional to the displacement x, and waiting until transients disappear, one can then observe frequency-response curves with jump-phenomena at saddle-node bifurcation points, see figure 1**b**).

These frequency-response curves have to be tracked fast in order to maintain constant internal parameters of the experiment. In general, thermal drift leads to changes in the separation s and therefore modifies the whole interaction yielding different time invariant sets, i.e. frequency-response curves. Consequently the control algorithm to track the solutions should be designed to operate completely on-the-fly without the need of expensive computations, that for example take place in common predictor-corrector pseudo arc length continuation schemes [14, 22]. By applying the Euler-Bernoulli beam theory on the micro cantilever one can obtain the tip dynamics described by coupling mechanical modes [30]. However, the first mechanical mode is dominating in most cases, therefore it is well established to model the dynamics of the tip in a rather simple damped driven harmonic oscillator with interaction forces as

$$\frac{\mathrm{d}}{\mathrm{d}t}x = v, \tag{1}$$

$$\frac{\mathrm{d}}{\mathrm{d}t}v = -\omega_0^2 x - \frac{\omega_0}{Q}v - \frac{\omega_0^2}{k}F_{TS}(x,v;s) + \tag{2}$$

$$\frac{\omega_0^2}{k}F\cos(\psi) \tag{3}$$

$$\frac{\mathrm{d}}{\mathrm{d}t}\psi = \omega_d \tag{4}$$

with cantilever angular eigenfrequency ω_0, cantilever oscillation quality factor Q, spring constant k, external forcing F, driving angular frequency ω_d, a tip-sample interaction force F_{TS}, which is generally unknown, and an initial condition $(x(0), v(0), \psi(0))^\intercal \in \mathbb{R}^2 \times \mathbb{S}_{[0,2\pi)}$. For convenience of an autonomous system we introduced the instantaneous phase ψ in the excitation signal, which changes at the rate of the driving angular frequency. Note that infinitesimal changes in ψ lead to continuous changes in the excitation signal, whereas deviations in the driving angular frequency itself would result in discontinuous excitation signals due to the product $\omega_d t$, which will be a key observation to later introduce control. Even though, we will not exploit the model for the continuation algorithm itself, we are going to use it for numerical validation.

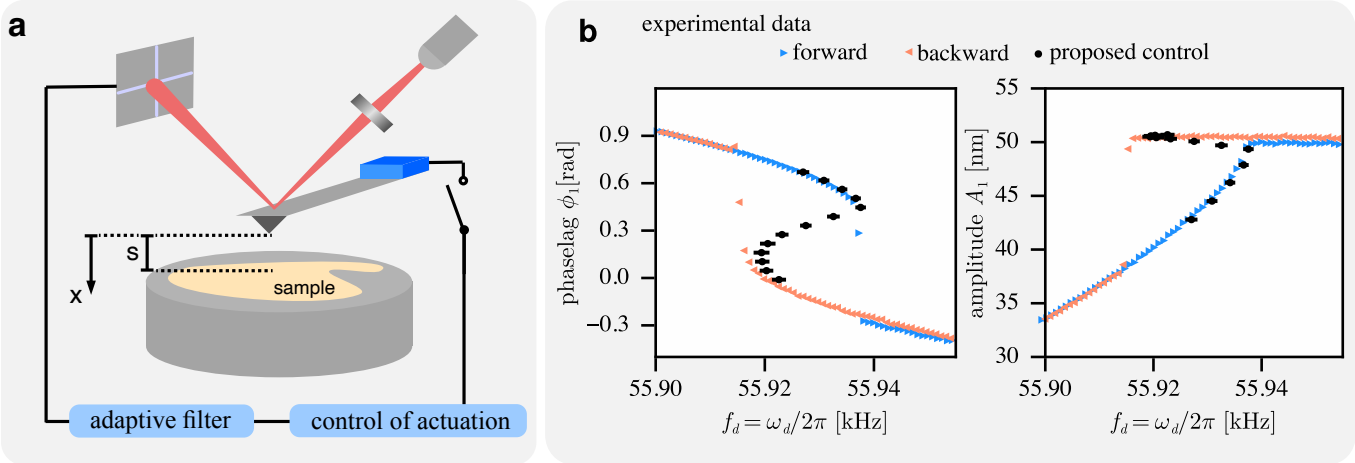

FIG. 1. **a** In dynamic mode atomic force microscopy a microcantilever is monoharmonically vertically driven. The deflection of the tip $x(t)$ is tracked by a laser deflection scheme and a segmented photodiode (position sensitive photodiode, PSPD). The nonlinear interaction can be changed by the nominal separation s. Using adaptive filters we can demodulate the deflection signal and can either feedback information back onto the actuation via control or just manually change the driving frequency. **b** By varying the driving frequency f_d and waiting until the transients are eliminated, experimental frequency-response curves (FRC), which display i.e. the fundamental phaselag ϕ_1 and amplitude A_1, can be obtained and clearly show bifurcation behavior. By use of control we are able to unveil the unstable branch experimentally.

B. Periodic orbits as steady states in a truncated Fourier space

The general issue within designing a control scheme that allows for tracking of unstable periodic orbits is to formalize the problem in such a way, that we can represent the targeted periodic orbit as a point. Feedback control towards a target point is then a well defined root finding or fixed point problem that can be solved by different techniques. From the analytical point of view, stroboscopic maps and therefore nonlinear control seem to be the most natural to use, since by design capture periodic orbits as fixed points. Indeed such control algorithms have been designed and show promising results for Duffing and Toda oscillators [29, 31]. Closely related is time delay control, which uses a time shifted output of a nonlinear system as a new actuation [32, 33]. A noise robust alternative is to project the dynamics of the tip $x(t)$ onto basis functions. Recently periodic B-Splines as a basis function set were proposed as an alternative to the typical Fourier approach [34]. Since we observe rather small deviations from elliptic orbits in experimental dynamic mode atomic force microscopy, we use the more common and traditional *Ansatz*

$$x(t) = \sum_{\omega_i \in \Omega} \left(X_{i,s} \sin \omega_i t + X_{i,c} \cos \omega_i t \right), \tag{5}$$

where the validity of (5) is given by the theorem of Fourier. In practice we focus, on a finite set $\Omega = \{\omega_i\}$, i.e. a truncated Fourier series, which approximates our signal $x(t)$ as $\tilde{x}(t)$. The general idea of truncation in Fourier space is spread across various disciplines, i.e. harmonic balancing [35, 36], van-der-Pol transformations [37] and rotating-wave approximations [38]. However, it is not straightforward to choose a suited set Ω due to nontrivial frequency conversions that take place in periodically forced nonlinear systems. As a result one should carefully investigate experimentally obtained time-series data and their respective frequency spectrum. In non-chaotic dynamic mode atomic force microscopy we observe a phase-locked behavior between the monoharmonic excitation signal $F \cos \omega_d t$ and cantilever deflection response $x(t)$ and additionally the presence of higher harmonics which motivates the *Ansatz* for an approximation $\tilde{x}$ of the tip dynamics

$$\tilde{x}(T,t) = \frac{1}{2} X_0(T) + \sum_{\omega_i \in \Omega} \left(X_{i,s}(T) \sin \omega_i t + X_{i,c}(T) \cos \omega_i t \right) \tag{6}$$

with $\Omega = \{n\omega_d | n, N \in \mathbb{N} : 0 < n \leq N\}$, that essentially represents a truncated Fourier series approach. We will refer to

$$X(T) = (X_0, X_{1,s}, X_{1,c}, \ldots, X_{N,s}, X_{N,c})^\intercal \in \mathbb{R}^{2N+1} \tag{7}$$

as the harmonic state, to $X_0, X_{i,s}, X_{i,c}$ as the harmonic variables, which change at a slow timescale $T \gg 2\pi / \min_i \omega_i$, and towards N as the truncation order. Note, that we are not inherently limited by a truncated Fourier series, *Zhou et al.* [39] also incorporated subharmonic resonances in their approximation, see equation (6). Since we are going to manipulate the driving frequency ω_d over time, but would like to obtain the harmonic state X based on the current actuation, we synchronize the clocks between actuation and Fourier

discretization by introducing the current instantaneous phase ψ in equation (6),

$$\tilde{x}(T,\psi) = \frac{1}{2}X_0(T) + \sum_{\psi_i\in\Psi}\left(X_{i,s}(T)\sin\psi_i + X_{i,c}(T)\cos\psi_i\right) \quad (8)$$

$$\frac{\mathrm{d}}{\mathrm{d}t}\psi = \omega_d \quad (9)$$

with $\Psi = \{n\psi \mid 0 < n \leq N \text{ with } n, N \in \mathbb{N}\}$ and $\psi(0) = 0$. One might think of this expansion as a projection onto a slow-fast dynamical system, in the rotating frame of the actuation, where we describe the fast oscillations by sine and cosines and the slow, transient behavior of the original system by the harmonic variables. If the finite set of frequencies Ω is sufficient and an equilibrium of the harmonic state X or equivalently a periodic orbit is reached, the harmonic variables are constant with respect to the slow timescale T and approximate the Fourier coefficients associated to the dynamics of the displacement of the tip. Therefore, we can formulate a root finding problem

$$\frac{\mathrm{d}}{\mathrm{d}T}X^\star(T;\mu) = 0 \quad (10)$$

to characterize the periodic orbit as an equilibrium point $X^\star \in \mathbb{R}^{2N+1}$. By changing a bifurcation parameter μ, in our case ω_d, adiabatically and demanding equation (10), one can obtain an $2N+1$ dimensional μ-response curve.

C. Nonlinear Frequency-Response Curves

Not only within the harmonic balancing, but also control-based continuation community one usually maps the truncated Fourier space to a collection of 1-dimensional curves by harmonic amplitudes A_i and phaselags ϕ_i

$$A_i(T) = \sqrt{\left(X_{i,s}(T)\right)^2 + \left(X_{i,c}(T)\right)^2}, \quad (11)$$

$$\phi_i(T) = \arctan_2(X_{i,c}(T), X_{i,s}(T)). \quad (12)$$

for each frequency ω_i in the set Ω. The $\arctan_2$ expression is thereby the inverse tangent function defined in all four quadrants. We would also like to emphasize, that even though these quadrature interpretations, see equations (11)–(12), are natural to choose to illustrate physically feasible quantities, there might exist alternative suitable maps

$$h\colon \mathbb{R}^{2N+1} \to \mathbb{R}, X \mapsto h(X), \quad (13)$$

that are computationally less demanding for actual hardware such as microcontrollers or field programmable gate arrays (FPGA) and still manifest in S-shaped (or Z-shaped) frequency-response curves and allow for easy to implement experimental tracking. Continuation schemes for S-shaped curves C can be viewed as a special case of natural parameter continuation. By effectively swapping the meanings of bifurcation parameter μ and observation $h(X)$, we can naturally parameterize the curve C by a grid of observations h. That is, we can reinterpret the bifurcation curve C as a single valued function. As a result $\mu(h(X^\star))$ is a single valued function in at least the neighborhood of interest $\mu \in [\mu_a, \mu_b]$. It is assumed that such a help function h can be constructed that fulfills this property. This allows for avoidance of arc-length continuation. Using a grid of targets G_h, that contain individual targets $h^\star$, and assuming $h(X^\star)$ follows an S-shape in the near resonance regime, we can aim towards one target $h^\star$ by a simple proportional plus integral control law

$$\frac{\mathrm{d}}{\mathrm{d}t}\psi = \omega_s + K_P(h(X(T)) - h^\star) + \lambda \quad (14)$$
$$\psi(0) = \psi_0$$

$$\frac{\mathrm{d}}{\mathrm{d}t}\lambda = K_I(h(X(T)) - h^\star) \quad (15)$$
$$\lambda(0) = 0$$

with a starting angular frequency ω_s, the current observation $h(X(T))$, the instantaneous phase ψ of the actuator, the integral part λ and real control gains K_P, K_I. Note that such control laws are non-invasive by design. If we reach our target $h^\star$ by choosing proper gains K_P, K_I and a steady-state of $h(X(T))$ is acquired with

$$\frac{\mathrm{d}}{\mathrm{d}t}\psi = \omega_s + \tilde{\lambda} = \omega_d \quad (16)$$

$$\frac{\mathrm{d}}{\mathrm{d}t}\lambda = 0, \quad (17)$$

one obtains again a monoharmonic excitation signal, but now reached the unstable periodic orbit characterized by $h^\star$. Note that phase-locked-loops (PLLs) are a special case of such control laws by using $h(X) = \phi_1(X)$. Indeed PLLs have been successfully used to stabilize unstable periodic orbits or extract backbone curves in experimental nonlinear dynamical systems [39–41]. Similar phase controls were established to reach unstable periodic orbits in the early 2010s [42, 43], which utilize analog phase shifters. However, latter are less versatile and more closely related to time-delay control. In our approach we can freely choose the map h, see (13).

D. Online Estimation of Harmonic State

A drawback of the control scheme acting in a truncated Fourier space is the inherent time delay between getting the harmonic state $X(T)$ and the true dynamics of the displacement $x(t)$. One way of solving this problem is to design the controller *offline* by tracking timeseries data $x(t)$ and applying a fast Fourier transform, between adaptations of the control signal, to gain information on the current observation $h(X(T))$. In fact, this would result in a time-splitting algorithm, that enables high precision but lacks convergence speed. Within engineering

or experimental sciences and digital signal processing one typically addresses this problem by estimating the harmonic variables online with a lock-in amplifier and hence multi order low-pass filters. By choosing suited cutoff frequencies at the low-pass filters one can reach a balance between convergence speed towards the harmonic state X and precision. An alternative that is known to outperform low-pass filters in convergence speed are Lyapunov-based estimators, which are common in adaptive filter theory [44] and were first used in a truncated Fourier space for noise canceling purposes by Widrow and Hoff [45]. Lately, they have also been introduced for demodulation in high speed atomic force imaging [46]. The fundamental idea relies on the linear parametric form of our truncated Fourier series, see equation (8). By introducing the basis vector

$$\begin{aligned} c(\psi) &= \left(\frac{1}{2}, \sin(\psi), \cos(\psi), \ldots, \sin(N\psi), \cos(N\psi)\right)^\intercal \\ &\in \mathbb{R}^{2N+1} \end{aligned} \tag{18}$$

and substituting $c(\psi)$ into equation (8) we arrive at a short linear parametric form of our current approximation $\tilde{x}$ of the displacement signal of the tip x

$$\tilde{x}(T, \psi) = X^\intercal(T) c(\psi), \qquad \frac{\mathrm{d}}{\mathrm{d}t}\psi = \omega_d, \quad \psi(0) = 0. \tag{19}$$

An online estimator for the harmonic state can now be constructed by manufacturing a Lyapunov-like function based on the current error $e(t) = x(t) - \tilde{x}(T, \psi)$ between measurement and estimation. Without further details, see [47, 48], one arrives at update equations for the harmonic state X that minimize the error $e(t)$ exponentially

$$\begin{aligned} \frac{\mathrm{d}}{\mathrm{d}t} X(T) &= \Gamma c(\psi)\Big(x(t) - X^\intercal(T) c(\psi)\Big) \qquad (20) \\ & \qquad X(0) = 0 \\ \frac{\mathrm{d}}{\mathrm{d}t}\psi &= \omega_d, \quad \psi(0) = 0, \qquad (21) \end{aligned}$$

where the diagonal matrix $\Gamma = \mathrm{diag}(\gamma_1, \gamma_2, \ldots, \gamma_{2N+1})$ represents individual stepsizes for each harmonic variable, that have to be chosen carefully and determine individual bandwidths. To ensure exponential convergence of the error $e(t)$ towards zero and therefore convergence of X, the basis vector c has to be persistently exciting, which is naturally given for a Fourier series approach, if the frequency set Ω is chosen adequately [47]. Note that the Widrow-Hoff learning rule or Least-Mean-Square (LMS) algorithm for online demodulation is a special case, where $\Gamma = \mathrm{diag}(\gamma)$ and an Euler forward time discretization $\xi(n\Delta t_{\mathrm{LMS}}) = \xi|_n$ is used

$$X|_{n+1} = X|_n + \gamma \Delta t_{\mathrm{LMS}} c(\psi|_n)(x|_n - X^\intercal|_n c(\psi|_n)). \tag{22}$$

We thus arrive at a computationally efficient scheme to approximate the current harmonic state X. A different path to obtain equation (22) is to define a Mean-Square error cost function and apply stochastic gradient descent. In the context of experimental continuation the Least-Mean-Square algorithm was first applied by *Abeloos et al.* [49].

E. Online Steady State Detection - Adapted Welford Algorithm

In order to gain the equilibrium of the harmonic state $X^\star$ and the associated bifurcation curve, we have to solve the zero-problem, see equation (10), and hence find fixed points of equation (22). This observation demonstrates the influence of the chosen adaptive filter to the total dynamics as well. The naive approach to determine $X^\star$ is to completely ignore the time derivative in the slow timescale T, see equation (10), and just assume that we always settle on $X^\star(T; \mu)$ after some constant time T_{wait} or constant number of iterations of the applied control law. Indeed, this solution is valid if we are able to approximate T_{wait}. However, such an approach tends to prolong sweeps of the bifurcation parameter μ, since the transient times between different setpoints $h^\star$ vary. In the specific case of dynamic mode atomic force microscopy this results in intolerable thermal drift and therefore different μ-response curves. Instead we use a different path and employ an adapted *Welford*'s algorithm [50] for a circular buffer that computes the current variance Σ as well as the average of the circular buffer (moving window) on-the-fly. Pushing new elements of the current observation $h|_n = h(X|_n)$ with a sampling frequency of $\frac{1}{\Delta t_{\mathrm{C}}}$ into the circular array of length L we obtain

$$\langle h\rangle|_{n+1} = \langle h\rangle|_n + \frac{h|_n - H}{L} \tag{23}$$

$$\begin{aligned} \Sigma|_{n+1} &= \Sigma|_n + (h|_n + H - \langle h\rangle|_n - \langle h\rangle|_{n+1}) \\ &\quad \times (h|_n - H) \end{aligned} \tag{24}$$

time explicit update equations for the average $\langle h\rangle$ and variance Σ of the circular buffer with head H, which contains the last stored entry, namely $h|_{n-1}$. We assume to have reached a steady-state of the harmonic state X and therefore fulfill equation (10) if the average of the observation is within some error bound $\Delta h^\star$ around the current target and additionally the standard deviation of the buffer is smaller than a given σ_{tol}.

$$\langle h\rangle|_{n+1} \in [h^\star - \Delta h^\star, h^\star + \Delta h^\star] \text{ and } \sqrt{\frac{\Sigma|_{n+1}}{L-1}} \leq \sigma_{tol} \tag{25}$$

The length L of the buffer as well as the as sampling frequency $\frac{1}{\Delta t_{\mathrm{C}}}$ should thereby be chosen to account for the slow-time scale $T \gg 2\pi/\min_i \omega_i$, hence $L\Delta t_{\mathrm{C}} \sim T$ where L should be at least ten. If conditions (25) are fulfilled, we effectively switch towards the next setpoint in the grid of targets G_h. For stability reasons it might be advantageous to choose finer grid distances at bifurcations points. Generally one should create such buffers for each individual harmonic variable in the harmonic

state to ensure minimal invasiveness. Nevertheless we assume, for computational efficiency, that convergence of the observation $h(X)$ is sufficient to identify a periodic orbit, since we raise the same assumption for the control itself. Hereby we conclude that, in contrast to PLL, where $h(X) = \phi_1(X)$, taking into account help functions or in other words observations, that consider further harmonic variables of the state X could be beneficial. The Welford algorithm not only allows for fast sweeps, due to individual transient times, but in principle also facilitates to calculate error bars on the bifurcation set, by tracking the bifurcation parameter μ, here ω_d, over time in a circular buffer as well, which is especially desirable in experimental setups. However, the adapted *Welford* algorithm comes with the cost of memory and assumes that the frequency set $\Omega = \{\omega_i\}$ is chosen sufficiently large in order for equation (22) to converge.

F. Explicit update Equations of the Controller

The overall dynamics can be ordered in three different timescales. First the position of the tip, and therefore the continuous time equations of motion, see equations (1), secondly the PI-controller, which is limited by the information gain of the harmonic state X and therefore the Least-Mean-Square (LMS) algorithm, see equation (22), and last the slowest time scale represented by filling the circular buffer with current observations and evaluating steady-state behavior, see equations (23)–(24). In experimental implementations the continuous time integral is replaced by the natural evolution of the physical system, whereas the control law and Welford algorithm have to be handled and accurately timed by processes implemented on the corresponding hardware, e.g. FPGA. In simulations we use an adaptive Runge-Kutta algorithm, namely *Tsit5()* of the open source Julia package *DifferentialEquations.jl* [51], to integrate the equations of motion. We use one periodic discrete callback with sampling time Δt_{LMS} to handle updates of the control law

$$\frac{\mathrm{d}}{\mathrm{d}t}\psi = \omega_s + u(t), \quad \psi(0) = \psi_0 \tag{26}$$

with starting angular frequency ω_s. Another periodic callback with sampling time Δt_{C} is employed, to update equations (23)–(24), of the circular buffer respectively. The transfer function of our simple controller can be written in the continuous s-domain as

$$G(s) = K_P + K_I\frac{1}{s} + K_D\frac{s}{sN_{\mathrm{low}}+1}, \tag{27}$$

where we optionally introduced a filtered differential part with timescale N_{low}. Applying a Tustin transform [52] and introducing the error $e|_n = h(X|_n) - h^\star$ at the timestep $n\Delta t_{\mathrm{LMS}}$, the time explicit PID control law $u|_{n+1} = p|_{n+1} + i|_{n+1} + d|_{n+1}$ can be evaluated by

$$\begin{aligned} p|_{n+1} &= c_1 e|_n && (28)\\ i|_{n+1} &= i|_n + c_2(e|_n + e|_{n-1}), && (29)\\ d|_{n+1} &= c_3(e|_n - e|_{n-1}) + c_4 d|_n, && (30) \end{aligned}$$

with initial conditions $p|_0 = 0, i|_0 = 0, d|_0 = 0$, where we introduced the constants

$$\begin{aligned} c_1 &= K_P && (31)\\ c_2 &= K_I\frac{\Delta t_{\mathrm{LMS}}}{2} && (32)\\ c_3 &= \frac{2K_D}{2N_{\mathrm{low}} + \Delta t_{\mathrm{LMS}}} && (33)\\ c_4 &= \frac{2N_{\mathrm{low}} - \Delta t_{\mathrm{LMS}}}{2N_{\mathrm{low}} + \Delta t_{\mathrm{LMS}}} && (34) \end{aligned}$$

for abbreviation and $p|_{n+1}, i|_{n+1}, d|_{n+1}$ are the proportional-, integral- and differential part respectively. N_{low} defines a time constant in order to smooth out the derivative of the differential controller. Generally the PID control can be further optimized by anti-windup features and sigmoidal activation functions between different targets $h^\star$. The positive gains $K = (K_P, K_I, K_D) \in \mathbb{R}^3_+$ are found by trial and error. From experience we advice to test proportional and integral gains around the natural frequency of the cantilever, which is in accordance to the stability analysis of a PLL-controlled Duffing oscillator [40]. For experimental implementations we suggest (depending on the actual hardware used) to use fixed-point arithmetic and binary angular measurements of ψ, for fast evaluation of the controller, see equations (28)–(30), and abusing overflow properties of the instantaneous phase over time, since numerical overflows can be used to naturally mimic the circular $\mathbb{S}_{[0,2\pi)}$ topology of the phase space. In order to comply with sinusoidal actuation, we should update the instantaneous phase at least ten times per period ($\Delta t_{\mathrm{LMS}} < \frac{2\pi}{10\omega_0}$). An experimental alternative might be to further smooth out the actuation signal given by the control law using an appropriate low-pass filter.

G. Limitations by Construction

By construction there are the following limitations:

1. By using a grid G_h of targets $h^\star$, we assume that the driving frequency $\omega_d(h(X^\star))$ is a single valued function in the near resonance regime. This is often expressed as an S-shape bifurcation set.

2. We assume that we can stabilize the formerly unstable periodic orbits using a simple PI-control. Although this allows for simple experimental implementations the control gains are for now only found by coarse estimates and systematic trial and error.

3. The effectiveness of the LMS algorithm to approximate the harmonic state $X(T)$ is strongly dependent on the sampling frequency of the deflection signal $x(t)$, as well as a sufficient frequency set $\Omega = \{\omega_i\}$.

III. RESULTS FOR VARIOUS INTERACTIONS

We will first demonstrate the feedback scheme on the well known Duffing or Kerr nonlinearity and mention the connections between the constructed experimental continuation algorithm, the mathematical framework of averaging and the stability of periodic orbits. Afterwards we will show stabilization of unstable branches in more pertinent tip-sample interaction forces, namely a Lennard-Jones with viscous damping and a Derjaguin-Muller-Toporov model.

A. Example I: Duffing/Kerr Nonlinearity

Within this subsection we consider the dynamical system

$$\begin{aligned} \frac{\mathrm{d}}{\mathrm{d}t}x &= v, \quad \frac{\mathrm{d}}{\mathrm{d}t}v = -\omega_0^2 x - \varepsilon c v - \varepsilon\alpha x^3 + \varepsilon F\sin(\psi) \\ \frac{\mathrm{d}}{\mathrm{d}t}\psi &= \omega_d, \end{aligned} \tag{35}$$

which is the well established forced Duffing oscillator with $\mathbb{R}^2 \times \mathbb{S}_{[0,2\pi)}$ phase space topology, soft excitation εF and damping εc [53]. In addition to the traditional interpretation of a nonlinear spring, one might think of an extremely simplified interaction model (1), which solely contains a repulsive, hardening $\alpha > 0$ or attractive, softening $\alpha < 0$ contribution. To analyze the forced system, see equation (35), we apply Krylov-Bogoliubov averaging [37]. Alternatively one can obtain the same results by the method of multiple scales, specifically the two-time method [53, 54]. We begin by selecting the fast-time variable ψ, representing the instantaneous phase, and slow-time variable $T = \varepsilon t$, which will describe the envelope time evolution. We will solely cover the case of near resonance driving $\omega_0^2 - \omega_d^2 = \varepsilon\Delta$, where $\varepsilon\Delta$ determines the detuning. By introducing the transformation

$$\begin{aligned} \begin{pmatrix} Y_{1,c}(T) \\ Y_{1,s}(T) \end{pmatrix} &= A \begin{pmatrix} x \\ v \end{pmatrix} \\ A &= \begin{pmatrix} \cos(\omega_d t) & -\frac{1}{\omega_d}\sin(\omega_d t) \\ \sin(\omega_d t) & \frac{1}{\omega_d}\cos(\omega_d t) \end{pmatrix}, \end{aligned} \tag{36}$$

and substituting the inverse transformation A^{-1} into equation (35) one obtains a coupled first order differential equation in the fast time scale t for the averaged sine and cosine quantities $Y_{1,s}, Y_{1,c}$. To obtain the slow-flow equations, see (37)–(38), one can afterwards average the system by integrating over one period $\int_0^{\frac{2\pi}{\omega_d}} \mathrm{d}t$ on both sides, as can be found in multiple textbooks e.g. [37], which yields

$$\begin{aligned} \frac{\mathrm{d}}{\mathrm{d}T}Y_{1,c} &= \frac{\varepsilon}{2\omega_d}\Big(-\omega_d c Y_{1,c} - \Delta Y_{1,s} - \\ &\qquad \frac{3\alpha}{4}Y_{1,s}(Y_{1,s}^2 + Y_{1,c}^2)\Big) \end{aligned} \tag{37}$$

$$\begin{aligned} \frac{\mathrm{d}}{\mathrm{d}T}Y_{1,s} &= \frac{\varepsilon}{2\omega_d}\Big(-\omega_d c Y_{1,s} + \Delta Y_{1,c} + \\ &\qquad \frac{3\alpha}{4}Y_{1,c}(Y_{1,s}^2 + Y_{1,c}^2) - F\Big). \end{aligned} \tag{38}$$

Frequency-Response curves can now be obtained by finding roots of the right hand side and varying ω_d. Note, that this procedure closely resembles our feedback scheme by setting the frequency set solely to the driving frequency $\Omega = \{\omega_d\}$. However, care has to be taken in comparing both results, since in the feedback-scheme the harmonic variables $X_{1,s}, X_{1,c}$ are, in contrast to the averaged quantities $Y_{1,s}, Y_{1,c}$, determined by a coupled fast-time ODE themselves, see equation (20), and therefore exist in a higher dimensional dynamical system. Generally one can also obtain stability information of the steady-states by linearization of the averaged ODE around the time invariant sets. Promising results on the stability of the closed-loop system, which combines the adaptive filter, the original system dynamics and a phase-locked loop were found by *Hippold et al.* [41], where nevertheless full information on the nonlinearity is assumed, which is naturally not given in experimental AFM settings. Instead, we choose parameters of the controller by trial and error. As an example of averaging as well as the constructed continuation scheme we analyze the forced Duffing system, see equation (35), with parameters listed in table I #1. In figure 2**a**) we showcase the ω_d-response curves, obtained by averaging and therefore essentially root finding of equations (37)–(38) and our proposed control. We notice small deviations between both results, since the first order averaging approach only accounts for the fundamentals, whereas the feedback scheme relies on the more generous frequency set $\Omega = \{0, \omega_d, 3\omega_d, 5\omega_d\}$. The control strategy was to target linearly decreasing phaselags $\phi_1^\star$ sequentially, which led to fast sweeps including the unstable branch. In fact, the control sweep was faster than open-loop sweeps due to close invariant sets along the sweep and shorter transients, since we actively manipulate the dynamics outside of invariant sets. In order to illustrate the multistability of the forced Duffing oscillator and grasp the difference between the time evolution of $(Y_{1,c}, Y_{1,s})^\intercal$ and the harmonic state X, we consider the driving frequency $\omega_d/\omega_0 = 1.65$ marked as a dashed line in figure 2**a**). The corresponding phase portrait of the averaged quantities is visualized in figure 2**b**). We can observe, that the slow-time vector field indeed has three time invariant sets, which represent three solutions on the frequency-response curves. The unstable solution is thereby topologically equivalent to a saddle-point and in a physical experiment not observable. To target the unstable solution, we effectively use polar co-

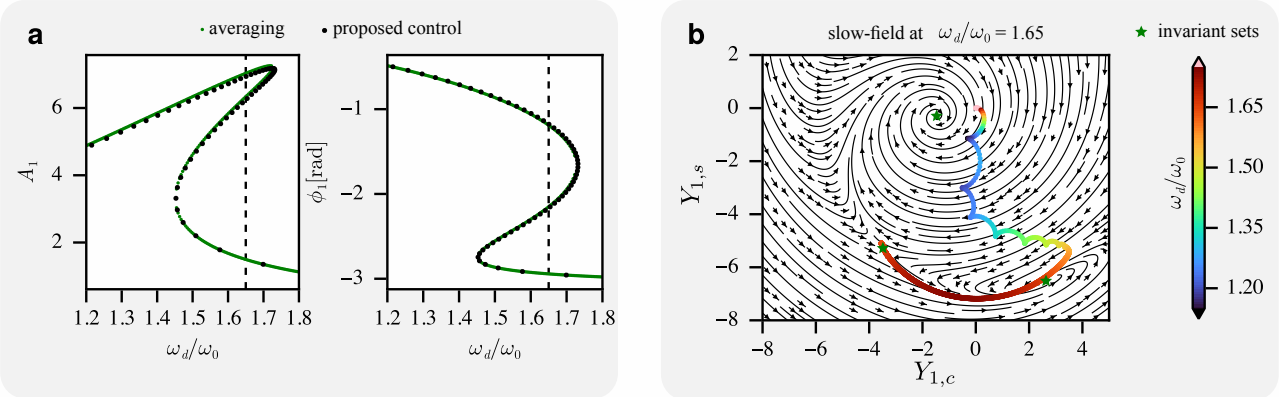

FIG. 2. On the left panel (**a**) we can see the fundamental amplitude A_1 and phaselag ϕ_1 for the averaged and controlled case of an repulsive Duffing oscillator for varying driving frequencies. Small deviations can be seen, due to the multiharmonic approach for the control. Panel (**b**) shows the slow-time vector field (37)–(38) at $\omega_d/\omega_0 = 1.65$. Furthermore we projected the transient of the proposed control for a single target $\phi_1^\star = -2.15$ [rad] onto the averaged phase space, the current driving frequency is used as color code.

ordinates to parameterize it by focusing on the angle. This can be considered as the fundamental phaselag target $\phi_1^\star = -2.15$ rad. To showcase, how the feedback control manipulates the dynamics of the displacement x and actuation in order to reach the formerly unstable time invariant set, we set up one initial condition $(x_0, v_0, \psi_0)^\intercal = (0, 0, 0)^\intercal$ with starting angular frequency $\omega_s = 1$ and target $\phi_1^\star = -2.15$ rad. The, by the LMS algorithm (22), estimated transient of the harmonic state $X(t)$ of the the displacement $x(t)$, is projected onto the slow-field, which approximates the open-loop behavior at $\omega_d/\omega_0 = 1.65$. The color code on the transient corresponds to the current driving angular frequency ω_d of the actuation. Interestingly, the control seems to be quite robust, despite being a simple PI-controller, since at similar driving frequencies (red colors) we effectively trespass another open-loop stable node-solution. We would like to highlight, that the LMS algorithm in this scenario is cold started ($X = 0$). In continuation sweeps, as in figure 2**a**), the distance between current and next harmonic states along the bifurcation curve $\|X^\star(T;\mu) - X^\star(T;\mu+\Delta\mu)\|$ is small, if the targets $h^\star$ are spaced accordingly, resulting in less elongated transients in the phase-space, since the LMS algorithm (22) has to adjust only slightly.

TABLE I. Parameters of the forced Duffing oscillator in the open-loop (system and adaptive filter) and additionally closed-loop system (system, adaptive filter and feedback). Parameters of the adaptive filter and feedback were found by trial and error.

#	ω_0	$\varepsilon\alpha$	εF	εc	γ	Ω_a	Δt_{LMS}	Δt_C	K_P	K_I	σ_{tol}
1	1	0.05	2.5	0.2	0.1	$\{1,3,5\}$	0.01	10.2	0.4	0.004	1e-4
2	1	1	14	1	0.1	$\{1,3,5\}$	0.05	5.2	10	1	1e-4

[a] in terms of harmonics and additionally the DC-part

To showcase the versatility of the algorithm we apply the continuation via feedback control on different Duffing parameters, see table I #2, and track the bifurcation diagrams of the higher harmonics in the frequency set Ω as well. In figure 3, we illustrated the complete bifurcation diagram for the fundamental and higher harmonic responses, achieved by manipulating the driving angular frequency ω_d by feedback-control with observation $h(X(T)) = \phi_1(X(T))$ and linearly spaced targets. We observe, that the continuation algorithm is able to not only track through stable periodic orbits, but also stabilizes formerly unstable time invariant sets beyond the saddle-node bifurcation points, indicated by black squares, with just one set of closed-loop parameters. On the left panel of figure 3(**a**–**b**) we see the fundamental amplitude and phaselag, respectively. The open-loop forward (blue) and backward (orange) sweeps as well as the control (grey) coincide for the stable branches of the system. In sub figure 3**a**) we display the closed-loop harmonic variables $X_{1,s}$ and $X_{1,c}$, which themselves would require pseudo-arc-length schemes. Due to the range $[-\pi, \pi)$ of $\arctan_2$ we colorize the top and bottom spines of the phaselag coordinate systems with green lines, indicating the periodic boundary behavior. On the right panel of figure 3(**c**–**f**) we illustrate the harmonic variables and parametrizations of the third and fifth harmonics. Since bifurcations occur on the more fundamental level of the system state and we try to capture the system state by the harmonic state X, we see saddle-node bifurcations at exactly the same driving frequencies for each element in Ω. We would like to highlight, that although we solely aim for a specific fundamental phaselag ϕ_1, we inherently continued the whole harmonic state X, since the Lyapunov estimator or discrete Least-Mean-Square filter combines all elements within the frequency set Ω into one estimation of the displacement $\tilde{x}|_n = X^\intercal|_n c(\psi|_n)$, effec-

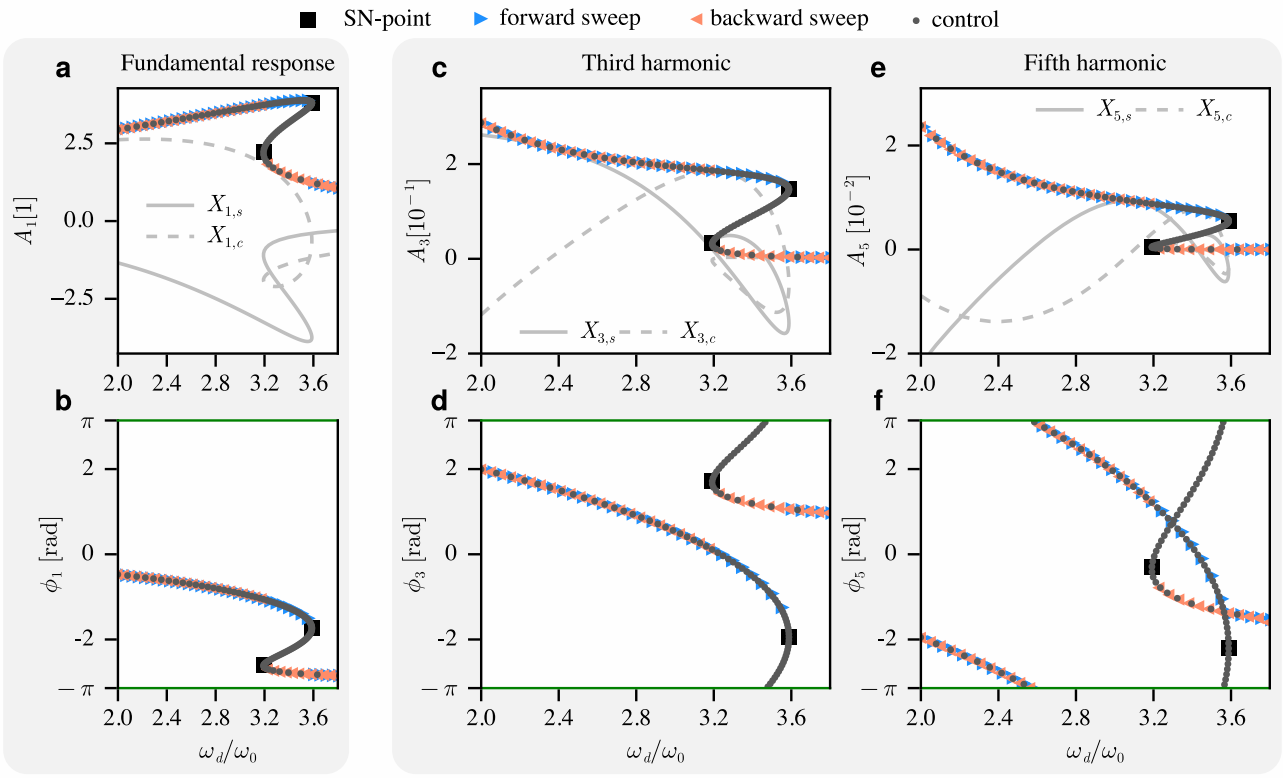

FIG. 3. Continuation of bifurcation diagram with feedback scheme on a Duffing oscillator with observation $h(X) = \phi_1(X)$ and parameters listed in table I # 2. Additionally we used a differential controller with $K_D = 2.5, N_{\text{low}} = 2.5$. The grey panel on the left (**a-b**) showcases the fundamental responses with saddle-node bifurcation points, forward- and backward open-loop sweeps and applied control. The harmonic variables in (**a**) do not describe a S-curve, however the observation ϕ_1 in (**b**) shows and is utilized as a set of targets. Although we only target at fundamental phaselags we intrinsically also reach the stable and unstable periodic orbits on the higher harmonic responses, see right grey panel (**c-f**), due to the coupling of the frequencies in the Lyapunov estimator.

tively coupling the dynamics of all harmonic variables over time, see equation (22). Interestingly, higher harmonic amplitudes, in contrast to A_1, also exhibit S-curves and might be used as a set of targets to manipulate the driving frequency accordingly. By considering an unwrap the higher order phaselags should also be suitable as an observation function $h(X)$. However the harmonic variables corresponding to the higher harmonics are orders of magnitude smaller and could be more vulnerable to noise in real experimental scenarios. With these polynomial nonlinearities in mind, we now focus on more relevant force microscopy contact models

B. Example II: Lennard-Jones model with viscous damping

One classical approach to model the interaction between tip and sample is by introducing a 12–6 potential, namely a Lennard-Jones interaction and supplement a viscous damping to account for nonlinear dissipation mechanisms [55]. The Pauli part is active in case of purely hardening, and the van-der-Waals part in purely softening. In reality both parts participate because of the finite oscillation amplitudes, striking both regimes. Though, for the attractive part a refined form was derived by Lifschitz, here we restrict ourselves to the Lennard-Jones. We hereby utilize dissipation introduced by introduced by [56], which translates in our coordinate system (1) and dynamical system to the tip-sample interaction

$$\begin{aligned} &F_{TS}(x, v; s) \\ &= \frac{12V_0}{\sqrt{(x-s)^2}}\left(\left(\frac{\sigma^2}{(x-s)^2}\right)^6 - \left(\frac{\sigma^2}{(x-s)^2}\right)^3\right) \\ &\quad + \frac{cv}{(s-x)^3} \end{aligned} \tag{39}$$

with potential height determined by V_0, potential minima distance proportional to σ, separation s and nonlinear damping coefficient c. Different Lennard-Jones models [56] respect the geometry of the sample and cantilever tip. Here we simply use the interaction between two pseudo particles. In the Derjaguin-Muller-Toporov

model, see subsection 3.3, we will take care of geometry by modelling the tip as a ball and the sample as a flat surface. From the experimental point of view it is also interesting how the frequency-response curve changes with respect to the separation s, which will serve in the following as a second bifurcation parameter. We account for different separations by applying the feedback scheme on several s and therefore construct a surface of all solutions in the (s, ω_d) domain, which include saddle-node and cusp-bifurcations [57].

TABLE II. Parameters of the forced Lennard-Jones oscillator with viscous damping in the open-loop system.

$\frac{\omega_0}{2\pi}$	Q	V_0	σ	k	c	s	F
[kHz]	[1]	[aJ]	[nm]	$[\frac{N}{m}]$	$[\mathrm{nN}\cdot\mathrm{nm}^2\cdot\mathrm{s}]$	[nm]	[nN]
55	400	4.2	2.8	0.7	$6\cdot10^{-4}$	60-120	0.3

TABLE III. Parameters of the forced Lennard-Jones oscillator with viscous damping in the open-loop (system and adaptive filter) and additionally closed-loop system (system, adaptive filter and feedback). Parameters of the adaptive filter and feedback were found by trial and error.

γ	Ω_a	$\frac{1}{\Delta t_\mathrm{LMS}}$ [kHz]	$\frac{1}{\Delta t_\mathrm{C}}$ [kHz]	K_P [kHz]	K_I [kHz/s]	σ_{tol} [rad]	L
0.05	$\{1,2,3,4\}$	687.5	3.6	22	0.22	$5\cdot10^{-6}$	40

[a] in terms of harmonics and additionally the DC-part

Our control-strategy is in this case to target 60 fundamental phaselags $\phi_1^\star$, for separations s between 60 nm and 120 nm. Generally one could achieve that in one single simulation, by changing the separation s after reaching all targets for a singular s. However, we are here opting for multiple simulations for each s, that can easily be computed in parallel. In experimental scenarios the former case might be favorable. Surprisingly, we were able to find parameters for the control algorithm by trial and error, that allowed to stabilize unstable periodic orbits for all here used separations, listed in table III. In figure 4(**a-b**) we see the various frequency-response curves of the fundamentals, leaning towards driving frequencies, since the nonlinearity acts predominantly attractive with our parameters. Within the blue regime, and therefore big separations, we effectively observe Lorentzians associated to the linear theory of damped driven harmonic oscillators. Moving towards smaller separations, at the black curves (approx. 90nm), we begin to see the existence of an unstable periodic orbit at a cusp-point, related to $\frac{\mathrm{d}\omega_d}{\mathrm{d}\phi_1} = 0$. At the most nonlinear red regime, we see in accordance to the experimental data a whole branch of unstable periodic orbits lying extremely close to the stable periodic solutions in the amplitude. However, in the fundamental phaselag they are well separated. We can summarize the multistability by projecting the saddle-node bifurcation points *a posteriori* in the (ω_d, s) domain, as seen in figure 4**c**), showcasing essentially a cusp-catastrophe. Since our feedback-scheme effectively continues the bifurcation curve for all frequencies in the set Ω, we now focus on one slice at constant separation $s = 65$ nm and analyze it more closely. Similarly, as with the multiharmonic approach to the Duffing oscillator, the higher harmonic frequency-response curves for the Lennard-Jones interaction can also be conceptualised. As illustrated in figure 5**a**), the amplitude of the unstable branch in the fundamental is nearly identical to that of the stable upper branch, further substantiating the assertion that pseudo-arc-length methods are not viable in the context of amplitude continuation. The same behavior is evident in the experimental data, as illustrated in figure 1. It is noteworthy that the unstable branches of the higher harmonics amplitudes are distinctly separated from the upper stable branch in magnitude, as illustrated in figure 5(**b-c**). It must be acknowledged, however, that amplitudes in the picometer regime may not be discernible in experimental frequency-response curves and, as a consequence, cannot be employed in arc-length schemes. Higher harmonic imaging is a prevalent technique within experimental dynamic mode atomic force microscopy. These numerical results suggest that at least bistability for certain driving frequencies should be observable in this context. Figure 5**d**) additionally plots the phase lags corresponding to the higher harmonics, which all show the S-curve property if unwrapped. Consequently, experimental higher harmonic phase contrast pictures of samples should indicate bimodal phase distributions for specific driving frequencies. We now focus on a different dynamic mode regime, often called tapping mode, in which repulsive forces are also quite relevant.

C. Example III: Derjaguin-Muller-Toporov (DMT)

Another more commonly used tip-sample interaction force in dynamic mode atomic force microscopy is the piecewise defined Derjaguin-Muller-Toporov (DMT) model, which results in our dynamical system (1) to the tip-sample force F_{TS}, conditionally depending on the instantaneous distance

$$\begin{aligned} x < s - a_0 &: \\ F_{TS}(x;s) &= \frac{HR}{6(s-x)^2}, \qquad (40) \\ x \geq s - a_0 &: \\ F_{TS}(x;s) &= \frac{HR}{6a_0^2} - \frac{4E}{3}\sqrt{R}\,(x-(s-a_0))^{\frac{3}{2}} \qquad (41) \end{aligned}$$

with the intermolecular distance a_0, Hamaker constant H, tip-radius R, separation s and effective elasticity module E. The Young modulus E is computed by individual elasticity modules $E_{t,s}$ of the tip and sample with respective poisson ratios $\nu_{t,s}$ by

$$\frac{1}{E} = \frac{1-\nu_t^2}{E_t} + \frac{1-\nu_s^2}{E_s} \qquad (42)$$

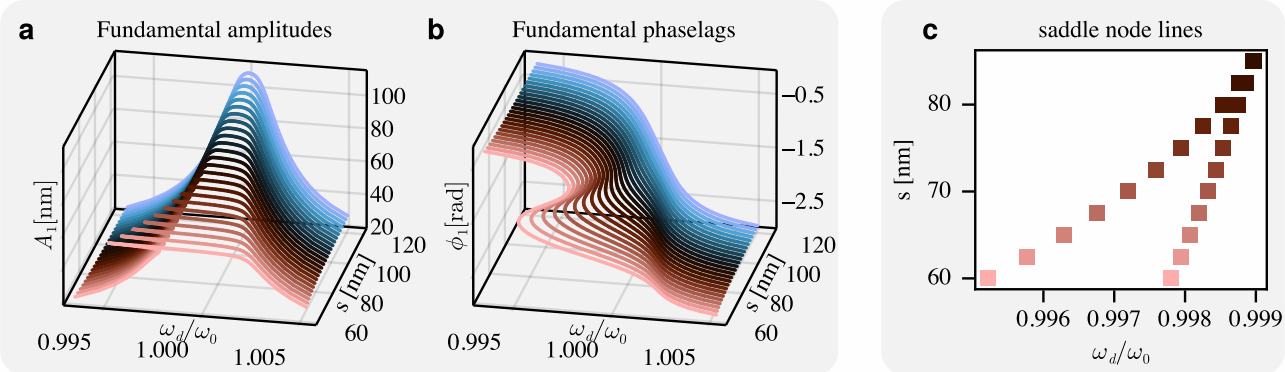

FIG. 4. Feedback-control applied to Lennard-Jones model with parameters listed in tables II-III. Illustrated in the left panel (**a-b**) are the fundamental amplitude A_1 and ϕ_1 for varying separations s, showing emergence of an unstable branch of periodic orbits for small s. On the right panel (**c**) we projected the saddle-node bifurcation points to the (ω_d, s)-domain and therefore effectively track the saddle-node lines *a posteriori*, highlighting regions of multistability.

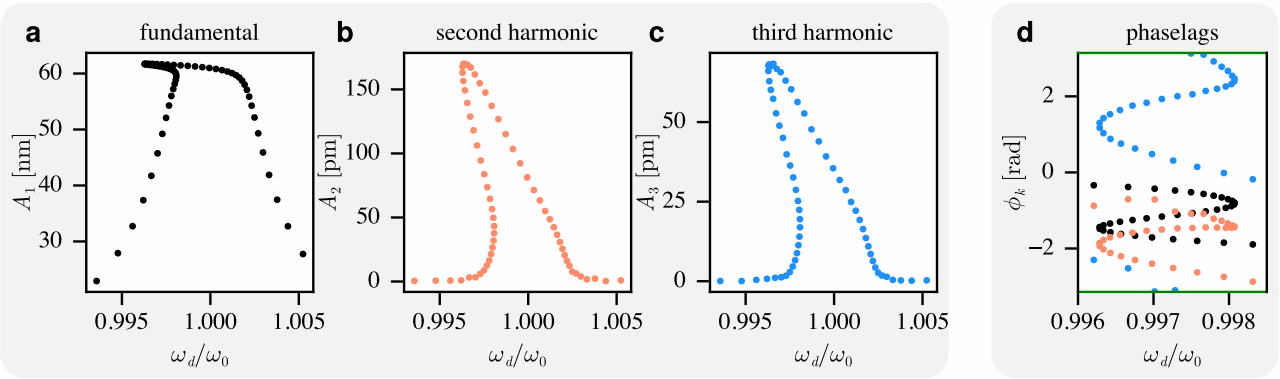

FIG. 5. Control algorithm applied to LJ model listed in tables II-III at constant separation $s = 65$ nm, indicating that we intrinsically track higher harmonic bifurcation curves. Panel **(a-c)** show the amplitudes of the respective harmonics. Using the same colors as in the left panel, we show in (**d**) the higher harmonic phaselags. The top and bottom spines are thereby green colored, indicating periodic boundaries, due to the range $[-\pi, \pi)$ of $\arctan_2$.

with $\nu_{t,s} = 0.3$, $E_t = 130$ GPa and $E_s = 1$ GPa. The DMT model allows for modelling elasticity and penetration into the sample. For benchmark purposes we here choose the same parameters as *Hoelscher et al.* [9] in the tapping regime of AFM, listed in table IV and apply the non-invasive feedback-control with parameters listed in table V for 20 different linearly spaced seperations s between 8.5 nm and 10.5 nm and 120 phase targets $\phi_1^\star$, which can be seen figure 6(**a-b**).

From a theoretical standpoint, the DMT tip-sample interaction (40)–(41) presents a more difficult challenge due to the fact that it is no longer differentiable for all displacements x. Nevertheless, the continuation algorithm should remain operational as long as the harmonic state $X(T;\mu)$ undergoes continuous variation in response to alterations in the bifurcation parameter μ, specifically ω_d,

TABLE IV. Parameters of the forced DMT-oscillator in the open-loop system. Parameters for the adaptive filter were found by trial and error.

$\frac{\omega_0}{2\pi}$ [kHz]	Q [1]	H [aJ]	k [$\frac{N}{m}$]	a_0 [nm]	R [nm]	F [nN]	γ	Ω_a
300	300	0.2	40	0.3	10	1.33	0.05	$\{1, 2, 3, 4\}$

[a] in terms of harmonics and additionally the DC-part

and the observation $h(X(T;\mu))$ remains S-shaped. As illustrated in figure 6(**a-b**), the construction of a manifold encompassing all solutions and the effective tracking of stable and unstable periodic orbits with identical control parameters for all separations s are indeed feasible and in accordance to *Hölscher et al.* [9]. Unstable solutions can

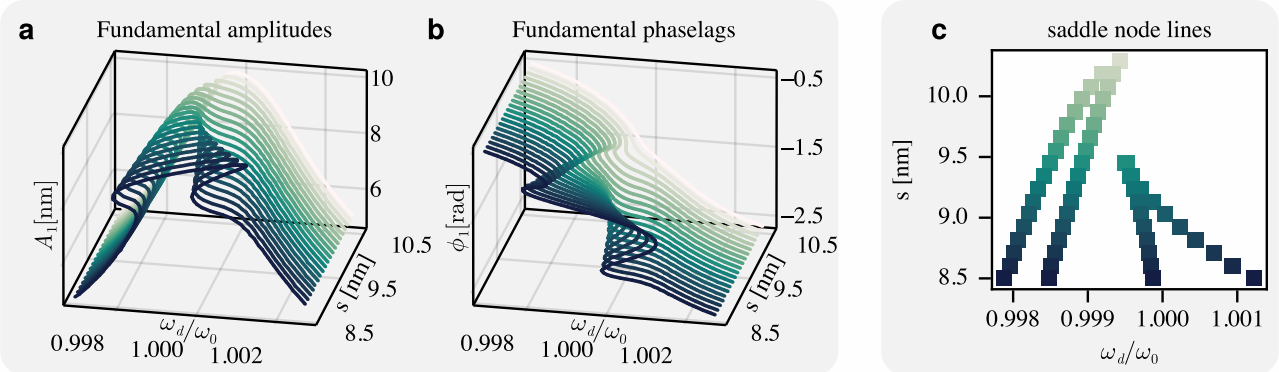

FIG. 6. Continuation algorithm applied to Derjaguin-Muller-Toporov model with parameters listed in tables IV-V. By utilizing the same control hyperparameters for all separations s we are able to stabilize the whole manifold of solutions, including stable and unstable branches, as can be seen in left panel (**a-b**). On the right panel (**c**) we projected the saddle-node bifurcation points to the (ω_d, s)-domain and therefore effectively track the saddle-node lines *a posteriori*, highlighting regions of multistability.

TABLE V. Closed-loop parameters for the forced Derjaguin-Muller-Toporov system.

$\frac{1}{\Delta t_{\mathrm{LMS}}}$	$\frac{1}{\Delta t_{\mathrm{C}}}$	K_P	K_I	K_D	N_{low}	σ_{tol}	L
[MHz]	[kHz]	[kHz]	[kHz/s]	[kHz · s]	[μs]	[rad]	[1]
6	30	1.6	480	0.3	6.66	10^{-5}	50

be characterized by $\frac{\mathrm{d}\omega_d}{\mathrm{d}\phi_1} < 0$, whereas saddle-node bifurcation points correspond to $\frac{\mathrm{d}\omega_d}{\mathrm{d}\phi_1} = 0$ and are projected in the (ω_d, s)-domain in figure 6**c**) encapsulating regions of multistability. The saddle-node points thereby merge in two distinguish cusp-points. A critical factor of experimental implementations is the natural frequency f_0 of the cantilever. By choosing fast cantilevers, we intrinsically need by the Nyquist limit high sampling frequencies if we want to track higher harmonics. In this specific example $\frac{1}{\Delta t_{\mathrm{LMS}}} = 6$MHz might be already located at the upper bound of experimentally realistic sampling frequencies.

IV. CONCLUSION AND OUTLOOK

We showed, that stabilization of unstable periodic orbits in dynamic mode atomic force microscopy is at least *insilico* possible by changing the driving frequency according to a non-invasive feedback-control scheme. Experimental implementations show promising results and first unstable solutions were shown in figure 1, but will be discussed in a different upcoming publication [10]. In section 2 we explained in detail the construction of the feedback-control experimentally as well as in simulations, introduced an adaptive filter to gain the harmonic state online and proposed a steady-state criterion to accelerate sweeps. Combining all three methods led to fast open-loop and closed-loop sweeps, which might inhibit problems arising by thermal drift in experimental settings. By applying these methods on numerical tip-sample interaction models in section 3, we concluded that inherent limitations of the feedback-control seem manageable and even work for different separations, manifesting in surfaces with unstable branches and cusp bifurcations.

Generally force microscopy experiments might be an excellent framework to challenge and test even more sophisticated experimental continuation algorithms, due to the easily adjustable nonlinearities, by changing the sample itself (or the medium) or by using different separations s. From the academic standpoint, such experiments can also be interesting due to still ongoing research in modeling tip-sample interactions, not only in the context of force microscopy, but also in tribology and electro-mechanic systems. Information on experimental, until now unreachable, unstable branches in dynamic mode atomic force microscopy can effectively be used to benchmark competing theoretical models, where unstable solutions can be obtained by various numerical software, e.g. [58–61]. Another point we would like to emphasize, is that in experimental settings numerous bifurcations can occur, we for now only took into account saddle-node bifurcations. Future *insilico* studies could revolve around control-based bifurcation analysis on liquid dynamic mode AFM models or different continuation strategies, for example working on a constant driving frequency, but changing the excitation amplitude.

V. DATA AND CODE-AVAILABILITY

Data and code used for the numerical examples can be found on Zenodo [62]. The pipelines to create shown figures with listed .csv files and Makie.jl [63] can also be found there.

ACKNOWLEDGMENTS

Funded by the Deutsche Forschungsgemeinschaft (DFG, German Research Foundation) SFB 1270/2 "Electrically active Implants" 299150580 and SFB 1477 "Light- Matter Interactions at Interfaces", project number 441234705.

[1] G. Binnig and H. Rohrer, Scanning tunneling microscopy, Surface Science **126**, 236 (1983).

[2] G. Binnig, C. F. Quate, and C. Gerber, Atomic force microscope, Physical Review Letters **56**, 930 (1986).

[3] D. Forchheimer, S. S. Borysov, D. Platz, and D. B. Haviland, Determining surface properties with bimodal and multimodal afm, Nanotechnology **25**, 485708 (2014).

[4] A. Chandrashekar, P. Belardinelli, M. A. Bessa, U. Staufer, and F. Alijani, Quantifying nanoscale forces using machine learning in dynamic atomic force microscopy, Nanoscale Advances **4**, 2134 (2022).

[5] S. L. Brunton, J. L. Proctor, and J. N. Kutz, Discovering governing equations from data by sparse identification of nonlinear dynamical systems, Proceedings of the National Academy of Sciences **113**, 3932 (2016).

[6] F. Jamitzky, M. Stark, W. Bunk, W. M. Heckl, and R. W. Stark, Chaos in dynamic atomic force microscopy, Nanotechnology **17**, S213 (2006).

[7] R. W. Stark, Bistability, higher harmonics, and chaos in afm, Materials Today **13**, 24 (2010).

[8] R. García, Dynamic atomic force microscopy methods, Surface Science Reports **47**, 197 (2002).

[9] H. Hölscher and U. D. Schwarz, Theory of amplitude modulation atomic force microscopy with and without q-control, International Journal of Non-Linear Mechanics **42**, 608 (2007).

[10] L. Böttcher, H. Wallner, N. Kruse, W. Just, I. Barke, J. Starke, and S. Speller, Exposing hidden periodic orbits in scanning force1 microscopy (2024), submitted.

[11] M. T. Cuairan, J. Gieseler, N. Meyer, and R. Quidant, Precision calibration of the duffing oscillator with phase control, Physical Review Letters **128**, 213601 (2022).

[12] E. Rull Trinidad, T. W. Gribnau, P. Belardinelli, U. Staufer, and F. Alijani, Nonlinear dynamics for estimating the tip radius in atomic force microscopy, Applied Physics Letters **111**, 10.1063/1.4991471 (2017).

[13] J. Sieber and B. Krauskopf, Control based bifurcation analysis for experiments, Nonlinear Dynamics **51**, 365 (2007).

[14] D. A. W. Barton and J. Sieber, Systematic experimental exploration of bifurcations with noninvasive control, Physical Review E **87**, 052916 (2013).

[15] M. Elmegård, B. Krauskopf, H. M. Osinga, J. Starke, and J. J. Thomsen, Bifurcation analysis of a smoothed model of a forced impacting beam and comparison with an experiment, Nonlinear Dynamics **77**, 951 (2014).

[16] S. Misra, H. Dankowicz, and M. R. Paul, Event-driven feedback tracking and control of tapping-mode atomic force microscopy, Proceedings of the Royal Society A Mathematical, Physical and Engineering Sciences **464**, 2113 (2008).

[17] C. I. Siettos, I. G. Kevrekedis, and D. Maroudas, Coarse bifurcation diagrams via microscopic simulators: A state-feedback control-based approach, International Journal of Bifurcation and Chaos **14**, 207 (2004).

[18] I. Panagiotopoulos, J. Starke, J. Sieber, and W. Just, Continuation with noninvasive control schemes: Revealing unstable states in a pedestrian evacuation scenario, SIAM Journal on Applied Dynamical Systems **22**, 1 (2023).

[19] A. Dittus, N. Kruse, I. Barke, S. Speller, and J. Starke, Detecting stability and bifurcation points in control-based continuation for a physical experiment of the Zeeman catastrophe machine, SIAM Journal on Applied Dynamical Systems **22**, 1275 (2023).

[20] I. de Cesare, D. Salzano, M. di Bernardo, L. Renson, and L. Marucci, Control-based continuation: A new approach to prototype synthetic gene networks, ACS Synthetic Biology **11**, 2300 (2022).

[21] D. Amakhin, A. Chizhov, G. Girier, M. Desroches, J. Sieber, and S. Rodrigues, Observing hidden neuronal states in experiments (2023), 10.48550/ARXIV.2308.15477.

[22] D. A. Barton, B. P. Mann, and S. G. Burrow, Control-based continuation for investigating nonlinear experiments, Journal of Vibration and Control **18**, 509 (2011).

[23] E. Bureau, F. Schilder, I. Ferreira Santos, J. Juel Thomsen, and J. Starke, Experimental bifurcation analysis of an impact oscillator—tuning a non-invasive control scheme, Journal of Sound and Vibration **332**, 5883 (2013).

[24] F. Schilder, E. Bureau, I. F. Santos, J. J. Thomsen, and J. Starke, Experimental bifurcation analysis—continuation for noise-contaminated zero problems, Journal of Sound and Vibration **358**, 251 (2015).

[25] S. Tatzko, G. Kleyman, and J. Wallaschek, Continuation methods for lab experiments of nonlinear vibrations, GAMM-Mitteilungen **46**, 10.1002/gamm.202300009 (2023).

[26] G. Raze, G. Abeloos, and G. Kerschen, Experimental continuation in nonlinear dynamics: recent advances and future challenges, Nonlinear Dynamics 10.1007/s11071-024-10543-9 (2024).

[27] Y. Li and H. Dankowicz, Model-free continuation of periodic orbits in certain nonlinear systems using continuous-time adaptive control, Nonlinear Dynamics **111**, 4945 (2022).

[28] S. Lenci, G. Rega, and L. Ruzziconi, The dynamical integrity concept for interpreting/ predicting experimental behaviour: from macro- to nano-mechanics, Philosophical Transactions of the Royal Society A: Mathematical, Physical and Engineering Sciences **371**, 20120423 (2013).

[29] N. Kruse, H. Wallner, A. Dittus, L. Böttcher, I. Barke, S. Speller, J. Starke, and W. Just, Large basins of attraction for control-based continuation of unstable periodic states, Nonlinear Dynamics **112**, 19809 (2024).

[30] A. Chandrashekar, P. Belardinelli, S. Lenci, U. Staufer, and F. Alijani, Mode coupling in dynamic atomic force microscopy, Physical Review Applied **15**, 024013 (2021).

[31] A. Dittus, N. Kruse, H. Wallner, L. Böttcher, I. Barke, S. Speller, J. Starke, and W. Just, Stroboscopic control and tracking of periodic states, Nonlinear Dynamics **112**, 1261 (2023).

[32] K. Pyragas, V. Pyragas, I. Z. Kiss, and J. L. Hudson, Stabilizing and tracking unknown steady states of dynamical systems, Physical Review Letters **89**, 244103 (2002).

[33] K. Pyragas, V. Pyragas, I. Z. Kiss, and J. L. Hudson, Adaptive control of unknown unstable steady states of dynamical systems, Physical Review E **70**, 026215 (2004).

[34] M. Blyth, K. Tsaneva-Atanasova, L. Marucci, and L. Renson, Numerical methods for control-based continuation of relaxation oscillations, Nonlinear Dynamics **111**, 7975 (2023).

[35] J. Košata, J. del Pino, T. L. Heugel, and O. Zilberberg, Harmonicbalance.jl: A julia suite for nonlinear dynamics using harmonic balance, SciPost Physics Codebases 10.21468/scipostphyscodeb.6 (2022).

[36] M. Krack and J. Gross, *Harmonic Balance for Nonlinear Vibration Problems* (Springer International Publishing, 2019).

[37] J. Guckenheimer, *Nonlinear Oscillations, Dynamical Systems, and Bifurcations of Vector Fields*, Applied Mathematical Sciences Ser. No. v.42 (Springer New York, New York, NY, 2002).

[38] C. Cohen-Tannoudji, J. Dupont-Roc, and G. Grynberg, eds., *Atom-photon interactions*, Wiley science paperback series (Wiley, New York, NY [u.a.], 2008) parallel als Buchausg. erschienen.

[39] T. Zhou and G. Kerschen, Identification of secondary resonances of nonlinear systems using phase-locked loop testing, Journal of Sound and Vibration **590**, 118549 (2024).

[40] V. Denis, M. Jossic, C. Giraud-Audine, B. Chomette, A. Renault, and O. Thomas, Identification of nonlinear modes using phase-locked-loop experimental continuation and normal form, Mechanical Systems and Signal Processing **106**, 430 (2018).

[41] P. Hippold, M. Scheel, L. Renson, and M. Krack, Robust and fast backbone tracking via phase-locked loops, Mechanical Systems and Signal Processing **220**, 111670 (2024).

[42] L. G. Villanueva, E. Kenig, R. B. Karabalin, M. H. Matheny, R. Lifshitz, M. C. Cross, and M. L. Roukes, Surpassing fundamental limits of oscillators using nonlinear resonators, Physical Review Letters **110**, 177208 (2013).

[43] H. K. Lee, R. Melamud, S. Chandorkar, J. Salvia, S. Yoneoka, and T. W. Kenny, Stable operation of mems oscillators far above the critical vibration amplitude in the nonlinear regime, Journal of Microelectromechanical Systems **20**, 1228 (2011).

[44] S. S. Haykin, *Adaptive filter theory*, 5th ed., Always learning (Pearson, Upper Saddle River, NJ, 2014).

[45] B. Widrow, J. Glover, J. McCool, J. Kaunitz, C. Williams, R. Hearn, J. Zeidler, J. Eugene Dong, and R. Goodlin, Adaptive noise cancelling: Principles and applications, Proceedings of the IEEE **63**, 1692 (1975).

[46] M. R. P. Ragazzon, M. G. Ruppert, D. M. Harcombe, A. J. Fleming, and J. T. Gravdahl, Lyapunov estimator for high-speed demodulation in dynamic mode atomic force microscopy, IEEE Transactions on Control Systems Technology **26**, 765 (2018).

[47] P. Ioannou, *Robust Adaptive Control* (Dover Publications, Incorporated, Newburyport, 2012) description based on publisher supplied metadata and other sources.

[48] M. R. Ragazzon, S. Messineo, J. T. Gravdahl, D. M. Harcombe, and M. G. Ruppert, Generalized lyapunov demodulator for amplitude and phase estimation by the internal model principle, IFAC-PapersOnLine **52**, 247 (2019).

[49] G. Abeloos, L. Renson, C. Collette, and G. Kerschen, Stepped and swept control-based continuation using adaptive filtering, Nonlinear Dynamics **104**, 3793 (2021).

[50] B. P. Welford, Note on a method for calculating corrected sums of squares and products, Technometrics **4**, 419 (1962).

[51] C. Rackauckas, A. Singhvi, Y. Ma, A. Thazhemadam, C. de Graaf, L. O. Hafner, M. Hatherly, S. P. Jones, dextorious, A. Strouwen, C. Caine, D. Widmann, E. Saba, H. Ranocha, Kvaz1r, M. G, Q. Qu, S. Isaacson, S. Olver, T. G. Badger, T. Vetter, c123w, J. Pelle, and M. Gwóźdź, Differentialequations.jl/7.13 (2024).

[52] A. V. Oppenheim and R. W. Schafer, eds., *Discrete-time signal processing*, 3rd ed., Prentice Hall signal processing series (Pearson, Upper Saddle River, 2010) literaturverz. S. 1082 - 1090. - With a companion website by Mark A. Yoder and Wayne T. Padgett.

[53] A. H. Nayfeh and D. T. Mook, *Nonlinear oscillations*, A @Wiley-Interscience publication (Wiley, New York [u.a.], 1979).

[54] R. H. Rand, Lecture notes on nonlinear vibrations (2012), https://hdl.handle.net/1813/28989, https://hdl.handle.net/1813/28989.

[55] B. Voigtländer, *Atomic Force Microscopy* (Springer International Publishing, 2019).

[56] W.-M. Zhang, G. Meng, J.-B. Zhou, and J.-Y. Chen, Nonlinear dynamics and chaos of microcantilever-based tm-afms with squeeze film damping effects, Sensors **9**, 3854 (2009).

[57] V. I. Arnol'd, *Catastrophe Theory*, 3rd ed. (Springer Berlin / Heidelberg, Berlin, Heidelberg, 2003) description based on publisher supplied metadata and other sources.

[58] E. Doedel, A. Champneys, T. Fairgrieve, Y. Kuznetsov, B. Sandstede, and X. Wang, Auto 97: Continuation and bifurcation software for ordinary differential equations (with homcont) (1999).

[59] A. Dhooge, W. Govaerts, and Y. A. Kuznetsov, Matcont: A matlab package for numerical bifurcation analysis of odes, ACM Transactions on Mathematical Software **29**, 141 (2003).

[60] A. Dhooge, W. Govaerts, Y. A. Kuznetsov, H. G. Meijer, and B. Sautois, New features of the software matcontfor bifurcation analysis of dynamical systems, Mathematical and Computer Modelling of Dynamical Systems **14**, 147 (2008).

[61] H. Dankowicz and F. Schilder, *Recipes for Continuation* (Society for Industrial and Applied Mathematics, 2013).

[62] L. Böttcher, H. Wallner, N. Kruse, W. Just, I. Barke, J. Starke, and S. Speller, Data: A method for stabilizing unstable periodic orbits in dynamic mode atomic force

microscopy (2025), code and data used in numerical examples.

[63] S. Danisch and J. Krumbiegel, Makie.jl: Flexible high-performance data visualization for Julia, Journal of Open Source Software **6**, 3349 (2021).